

# Weakly-Supervised Learning via Multi-Lateral Decoder Branching for Guidewire Segmentation in Robot-Assisted Cardiovascular Catheterization

Olatunji Mumini Omisore<sup>1</sup>, Toluwanimi Akinyemi<sup>1</sup>, Anh Nguyen<sup>2</sup>, Lei Wang<sup>1</sup>

<sup>1</sup>Shenzhen Institute of Advanced Technology, Chinese Academy of Sciences, Shenzhen, China

<sup>2</sup>Department of Computer Science, University of Liverpool, Liverpool, United Kingdom

**Email for correspondence:** [omisore@siat.ac.cn](mailto:omisore@siat.ac.cn)

**Abstract.** Although robot-assisted cardiovascular catheterization is commonly performed for intervention of cardiovascular diseases, more studies are needed to support the procedure with automated tool segmentation. This can aid surgeons on tool tracking and visualization during intervention. Learning-based segmentation has recently offered state-of-the-art segmentation performances however, generating ground-truth signals for fully-supervised methods is labor-intensive and time consuming for the interventionists. In this study, a weakly-supervised learning method with multi-lateral pseudo labeling is proposed for tool segmentation in cardiac angiograms. The method includes a modified U-Net model with one encoder and multiple lateral-branched decoders that produce pseudo labels as supervision signals under different perturbation. The pseudo labels are self-generated through a mixed loss function and shared consistency in the decoders. We trained the model end-to-end with weakly-annotated data obtained during robotic cardiac catheterization. Experiments with the proposed model shows weakly annotated data has closer performance to when fully annotated data is used. Compared to three existing weakly-supervised methods, our approach yielded higher segmentation performance across three different cardiac angiogram data. With ablation study, we showed consistent performance under different parameters. Thus, we offer a less expensive method for real-time tool segmentation and tracking during robot-assisted cardiac catheterization.

**Keywords:** Cardiovascular interventions, weakly-supervised learning, Multi-lateral decoder branching, Segmentation, Robot-assisted catheterization.

## 1 Introduction

As a major cause of morbidities and mortalities, cardiovascular diseases have received a significant amount of attention [1]. Currently, intelligent surgical robots and advanced imaging methods are adopted for intervention of cardiovascular diseases to prevent the challenges associated with open surgery. This includes the use of X-ray, computed tomography, magnetic resonance imaging for endovascular catheterization and evaluation procedures [2]. Medical imaging modalities allow for non-invasive inspection and visualization of the cardiovascular system during computer-assisted diagnosis, planning, and treatment. At each stage, cardiac angiograms are acquired

while advanced image processing methods are required for structural interpretation and quantification [3]. Thus, accurate fast and accurate image processing methods are helpful for tool tracking and visualization during cardiovascular interventions. The image processing involves registration, segmentation, or reconstruction of flexible endovascular tools and vessels in the cardiac angiograms. On segmentation, different *physics-* and *learning-based* methods have been developed. Classically, *physics-based* methods are used to categorize the cardiac structures in grayscale or RGB images through pixel-level intensity thresholding or region clustering. These often involve manual tasks such as bounding box generation to reduce computational complexities. Therefore, it may not be suitable for clinical applications with large and dynamic data.

Learning-based segmentation have aided some progresses for cardiovascular angiogram analytics [4, 5]. With initiative of fully-supervised learning, Zhou *et al.* [6] developed the concept of pyramid attention recurrent networks for tool segmentation and tracking in x-ray images. Ronneberger *et al.* [7] proposed U-Net, an architecture that utilize contracting and expanding paths for precise pixel-level segmentation and localization in medical imaging. The architecture was extended with nested dense skip paths and deep supervision for more powerful medical imaging applications [8]. The learning-based models are capable of capturing fine grained details of foreground pixels at low level resolution. However, the models are less sensitive to boundary preservation. To resolve this, Gu *et al.* [9] developed context encoder network to capture high-level information for preservation of spatial details in medical image segmentation. However, the network model could only outperform classical U-Net in retina disc segmentation and lung segmentation [9, 10]. The learning-based methods greatly improved segmentation accuracy in medical imaging. However, obtaining a generalized model for dynamic imaging data with distribution mismatch and class imbalance is hard [11]. The networks only consider local feature contexts and incur performance and overhead issues to solve this challenge. Thus, such network cannot utilize long range dependencies in sequential data as in cardiac angiograms. Overall, fully-supervised learning places huge burden of creating quality masks on surgeons.

Weakly-supervised learning methods can enhance medical image processing in computer-assisted interventions [12-14]. The strategies can eliminate the challenges associated with developing generalized fully-supervised learning models. Rather than relying on dense annotation, weakly-supervised methods are used to train neural network models with sparse or partial annotation signals. These can be generated with reduced time and effort of the domain experts. Currently, point-wise, scribble-wise and bounding box labels have been proposed for model training [12]. Qu *et al.* [15] developed a weakly-supervised segmentation model with partial point-wise annotation. As a two-stage segmentation framework, it consists of a self-supervised model with Gaussian masking for detecting nuclei locations. He *et al.* [16] utilized a self-teaching strategy for pixel-level semantic segmentation in sparsely annotated 2D cardiac images. These techniques are based on training model with either sparsely-annotated data or mixing few fully-annotated signals with huge unlabeled portion to gain feature maps for comparable segmentation output as when using fully-supervised methods. Viniavskyi *et al.* [17] trained a supervised model to generate image-level pseudo labels of abnormal chest regions in X-ray images, and propagated activation maps for automated localization of abnormal regions in the images. The model has dual output branches that predict a displacement vector field and class boundaries [17].

Bounding-box was widely used prior to advent of learning-based segmentation [18, 19]. Its application for developing generalized and robust weakly-supervised learning models have also received significant attention. Typically, it involves using three or more coordinates around an object of interest in a given image, and training a learning model for boundary detection. It is well applied in different areas of medical imaging [13, 14, 20, 21]. Determining a certain region-ground separation for bounding boxes is a major challenge since there is no supervisory signal. Scribble-based methods are actively being investigated for weakly-supervised semantic segmentation in medical imaging. Luo *et al.* [12] showed how scribbles can be used for weakly-supervised learning and segmentation of 13 abdominal organs. Scribble annotations can enhance state-of-the-art learning-based architectures like U-Net, U-Net++, and DeepLabV3+ which are commonly used for medical image segmentation. Furthermore, scribble-based supervision signals could lean on weakly-supervised learning with global regularization, multi-scale attention and mixed augmentation consistency methods [22-24] to improve segmentation performance in cardiovascular angiograms. This can reduce the burden of generating dense annotation needed for fully-supervised learning, and offer close segmentation outputs. Alternatively, weak supervision can be done with point annotations in medical images. In addition to Qu *et al.* [15], Zhai *et al.* [25] applied point annotation for weakly-supervised learning in medical image processing. However, only a few point masks were used to define the segmentation targets. Also, the study applied contextual regularization with conditional random field and variance minimization for consistency learning [22]. Issam *et al.* [26] showed that single pixel annotation with consistency learning can regularize segmentation outputs that are stable with input images in weakly-supervised learning. Point annotation is easier and faster compared to the scribble and bounding-box methods however, the existing works have not indicated it to relieve experts' burdens of obtaining a huge amount of segmentation masks as the entire pixels of interest were masked in the currently available works.

Learning via sparse annotation is challenging and needs regularization. Thus, application of existing weakly-supervised models and annotation methods is limited in cardiovascular catheterization imaging. Yang *et al.* [27] used voxel labels generated by line filtering and updated in iterative training cycles to obtain class activation feature maps for catheter segmentation. The study utilized bounding-box annotation. This yielded noisy masks with model whose performance is far-fetched from state-of-the-art fully-supervised models. Also, it is not applicable for segmenting endovascular tools when assuming deformable shapes as usually occur during catheterization.

In this study, a novel weakly-supervised learning method is proposed for concurrent pixel-level pseudo labeling and guidewire segmentation in cardiovascular angiograms. The proposed method involves optimizing architecture of the existing backbone networks with single encoder and multiple decoders, to learn from scribble annotations for pixel-level segmentation. The decoders' structures are perturbed to learn complementary features, and imposed with shared-consistency regularization to obtain a robust and well-generalized segmentation model. The method is implemented in U-Net architecture with one encoder and multi-lateral branched decoders. The multi-scale pixel-wise predictions are regularized with a combined loss function that generates pseudo labels used for end-to-end model training. The network was applied for guidewire segmentation in synthesized human angiogram data, which is publicly

available [28], and those obtained during robot-assisted cardiovascular catheterization in rabbit and pig [29]. The main contributions of this study are to develop a: 1) weak supervision technique with multi-lateral branched decoders for partially-annotated guidewire segmentation in cardiovascular angiograms; 2) shared-consistency term for enhancing the self-generated supervision signals from the multiple decoders; and 3) experimental studies to show that our proposed method offers stable, accurate and consistent segmentation performance on three different angiogram data sets.

## 2 Proposed Method

We utilized angiogram dataset with partial annotation to exploit relevant knowledge of domain experts. With assumption that data instances are drawn from a Gaussian mixture model  $\mathcal{J}(x|\theta) = \sum_{i=1}^n \beta_i \mathcal{J}(x|\theta_i)$  with  $n$  classes, soft pseudo labels can be concurrently generated and propagated for training network parameters. Where  $\beta_i$  is a mixture coefficient such that  $\sum_{i=1}^n \beta_i = 1$ , and  $\theta = \{\theta_i\}$  are the network parameters. However, there is need to compare pixels in the partial annotations with the unlabeled components in an angiogram to determine their class. First, we consider label  $y_i$  of pixel  $i$  as a random variable whose distribution  $P(y_i|x_i, g_i)$  can be determined by the mixture component  $g_i$  and feature vector ( $x_i$ ) representation of the pixel. With maximum *a posteriori criterion*, a model that utilizes the supervised signals to estimate  $y_i$  for unlabeled sets can be formulated as Eq. 1, where  $P(g_i = j|x_i) = \frac{\beta_j \mathcal{J}(x|\theta_j)}{\sum_{i=1}^n \beta_i \mathcal{J}(x|\theta_i)}$ . The task is to use the limited annotated pixels to estimate class distributions of unlabeled components. The estimated signals can be extended to improve the model’s performance beyond the supervised learning stage. We present this as performing two step training where the first is to generate pseudo labels from available annotations in a supervised manner. The pseudo labels are derived as a mean prediction from multi-lateral decoders in the first step, and subsequently combined with the original annotations to concurrently train the model.

$$h(x) = \underset{c \in [0,1]}{\operatorname{argmax}} \sum_{i=1}^n P(y_i = c | g_i = j, x_i) \times P(g_i = j | x_i) \quad (1)$$

### 2.1 Self-generating Pseudo Labels

As shown in Figure 1, the weak-supervision model is based on encoder-decoder structure with one encoder feeding multiple branches of decoders that uses different dilation rates for abstracting multi-scale feature maps. Upon initializing the training class distributions from the annotated signals, outputs from the model’s auxiliary decoders can be used to generate quasi labels by learning from the available supervision signals. The feature maps from the encoder are passed through the lateral decoder branches while the outputs can be combined to form the pseudo labels.

**Learning from Annotated Pixels.** The training data consists of angiogram images with partial annotations. This labeling approach includes a set of pixels with known and unknown labels. The annotations are used for network training by minimizing a

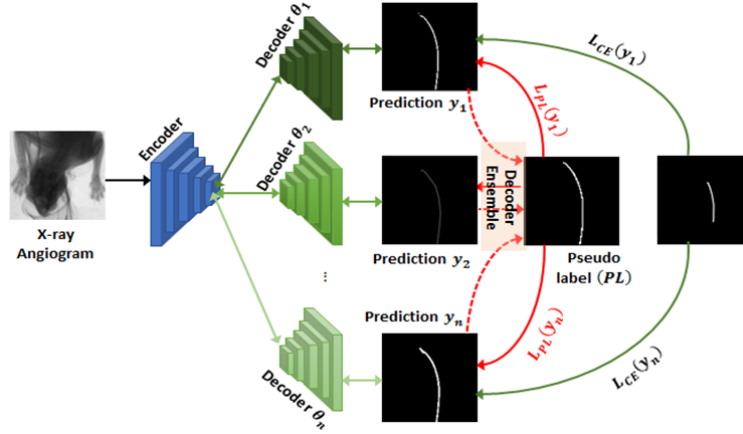


**Fig. 1.** Framework of weakly-supervised learning model with an encoder and laterally-branched multiple decoders. The decoders integrate perturbed and actual feature maps for quasi-labeling and segmentation of guidewire pixels in angiograms, respectively.

loss function with assumption that one-hot class values  $\hat{Y} := \mathcal{H}(x|\theta)$  is an estimate of the ground-truth ( $Y$ ). During training, network parameters  $\theta_{\mathcal{H}}$  are learnt to minimize model loss with the cross-entropy function  $\mathcal{L}_{CE}(y, s := g_i|x_i) = \sum_c \sum_{i=1}^{len(s)} \log(y_i^c)$ ; where  $s$  are one-hot annotation represented via the mixture component  $g_i$  and features ( $x_i$ ), and  $y_i^c$  is the probability that  $i^{th}$  pixel belongs to class  $c$ . Since angiograms are partly annotated, pseudo labels are generated to simulate fully-supervised learning.

**Generating Pseudo Labels.** The model uses multiple lateral decoders to propagate available annotated pixel across unlabeled pixels in angiograms. For this, each decoder instance independently utilize feature maps extracted from the encoder to self-generate pseudo labels. One decoder is designated as the main decoder and used to produce the actual pixel-level segmentation. Supervision signals from the main decoder are combined with the outputs of the auxiliary decoder(s) to generate pseudo labels. The probability maps are mixed as  $PL(Mix_{\lambda}) = \text{argmax} \sum(\lambda^{d=1, \dots, K}) \times y_i^c$ , where  $\lambda$  is a random value, chosen between 0 and 1 in each iteration, to penalize the outputs of the decoders. It is selected such that  $\sum_{d=1}^n \lambda^d = 1$ . Feature maps with increased diversity are obtained by perturbing the outputs from the auxiliary decoders. The perturbation is implemented as stochastic forward passes with random dropout and propagated across the training iterations [30, 31]. This provides subsamples of the original model  $\mathcal{H}(y_i, \mathcal{J}(x|\theta))$  with randomly dropped features ( $\theta_i$ ). Thus, the pseudo labels obtained from unlabeled pixels are added as new supervision signals to supplement the training signals. However, random perturbations on auxiliary decoders cause supervision signals from the unlabeled set to be noisy. Thus, pseudo labels from the differently perturbed decoders are inconsistent and would make the sub-models to possess variations in their characteristics. Hence, it is necessary to ensure consistency amongst the decoder outputs to filter pseudo labels for refined model training.

## 2.2 Training with Shared Consistency

Outputs from the multiple decoders are aggregated to be more robust than a model with using single decoder. This is approached by mixing the pseudo labels generated from the decoders with shared consistency for reliable training [32]. Given a scenario with annotated labels  $\mathcal{D}_L = \{x_i, y_i\}_{i=1}^k$  and pseudo labels  $\mathcal{D}_p = \{x_i, y_i\}_{i=k+1}^l$ , the overall training is modeled with respect to all labels as:  $\min_{\theta} \sum_{i=1}^l \mathcal{L}_{sup}(\mathcal{J}(x|\theta), y_i) + \sum_{i=1}^{l+n} \mathcal{L}_{pse}(\mathcal{J}(x; \theta, y_i), \mathcal{J}(x; \theta', y_i'))$ , where  $y_{i,\dots,k}$  and  $y_{k+1,\dots,l}$  are ground-truth and self-generated labels, respectively. The objective function includes using binary cross-entropy loss ( $\mathcal{L}_{sup}$ ) for supervised loss minimization obtained with the ground-truth. The other part involves training the model on pseudo labels generated with Softmax learning and a mean consistency loss ( $\mathcal{L}_{pse}$ ). This will normalize the variations caused by applying different perturbations in the distinct auxiliary decoders. A consistency control parameter ( $\gamma$ ) is used to regulate the pseudo labels. Restricting the pseudo labels and using multiple decoders (3 or more) offers strong supervision signals and reduces mislabels during training. Thus, pairwise pseudo label supervision is utilized. For a given pair of any two decoders with pseudo labels ( $PL_{d1}, PL_{d2}$ ), the label signals obtained from  $PL_{d1}$  is used to supervise the signals from  $PL_{d2}$  as given in Eq. 2.  $\mathcal{D}(\cdot)$  is a distance measure between the class label distributions in the two groups. This provides shared consistency such that the different sub-model can co-learn as the decoders learn together. Thus, the variation amongst the decoders' outputs will be very small, and that can facilitate model consistency. The final combined loss (Eq. 3), which includes weighted sum of segmentation loss added to an aggregated regularized loss for model's consistency, was utilized for weakly-supervised model training.

$$\mathcal{S}(PL_{d1}, PL_{d2}) = \frac{1}{K} \cdot \frac{1}{|\mathcal{D}_U|} \sum_{x_i \in \mathcal{D}_U} \left( \sum_{d=1}^K \mathcal{D}(g(\theta), g(\theta')) \right) \quad (2)$$

$$\mathcal{L}_{all} = \frac{1}{K} \left( \mathcal{L}_{pCE}(y_{d=1}, s) + \sum_{d' \forall d > 1}^K \mathcal{L}_{pCE}(y_{d'}, s) \right) + \gamma \times \left( \sum_{\substack{\forall \{d1, d2\} \\ \ni K}}^K \mathcal{S}(PL_{d1}, PL_{d2}) \right) \quad (3)$$

## 3 Experiment Results and Evaluation

The performance of proposed method was validated on private and public cardiac angiogram datasets and compared with fully-supervised and three existing weakly-supervised learning methods. Performances were reported base on mean intersection-over-union (mIoU). For the private data sets, robot-assisted catheterization trials were performed in four rabbits (*weight*:  $2.21 \pm 0.29$  kg) and a pig (*weight*: 35.1 Kg). The auricle-to-coronary artery and femoral-to-cardiac vascular paths were cannulated in the animals, respectively. Institution ethical approvals were obtained AAS-191204P and SIAT-IRB-190215-H0291, respectively, and the procedures were carried out with our existing RCS platforms [1, 19, 29]. Fluoroscopy sequences were recorded and each angiogram is projected as an image frame of  $1440 \times 1560$  pixels with resolution of

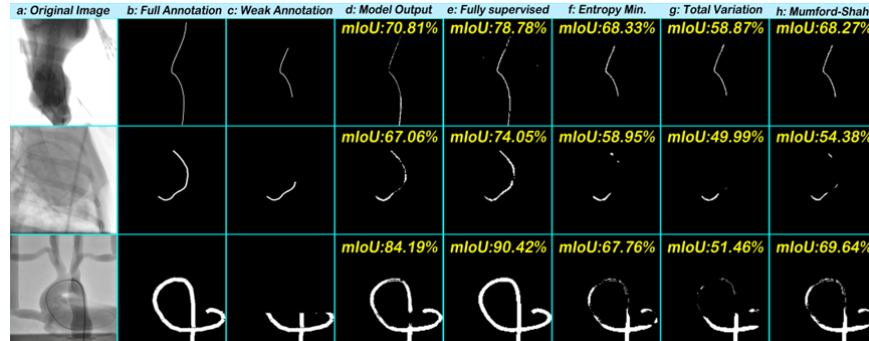


**Fig. 2:** Segmentation results for selected frames in the test sets of three different data [28, 29]. **a)** original angiograms, **b)** fully annotated frames, and **c)** partial-annotated images. Outputs of **d)** proposed method, **e)** fully-supervised method, and **f-h)** existing weakly-supervised methods.

$1.8 \times 1.8 \text{ mm}^2$ . A publicly available data set [28], each frame with a size of  $256 \times 256$ , was also used to validate the model. In all the datasets, 50% of guidewire pixels in the frames were annotated with LabelMe [29], and directly used to implement the network.

### 3.1 Implementation Details and Results

The segmentation model is implemented on a modified U-Net backbone [33]. The base model was extended to have three decoders with the first one serving as the main decoder. The other two are auxiliary decoders used for generating pseudo labels from the weakly-annotated data. The auxiliary decoders are replicas of the main decoder with addition of convolution and dropout layers. Thus, different feature maps are obtained from the three decoders, which help to prevent model overfitting. The model was implemented in Tensorflow Keras® and validated with the data mentioned above. For training optimization, the image intensity was normalized, and data augmentation steps: zooming (0.2), translation (0.2), shearing ( $45^\circ$ ), rotation ( $45^\circ$ ), and flipping (0.5) were done. The model was trained on Nvidia A6000 RTX GPU for 200 epochs. Each data set was split into 80% to train and validate the model in a 9:1 ratio, and 20% to test the model. Adam optimizer with initial learning rate of  $10^{-4}$  was used to minimize Eq. 3 where  $\gamma$  was set as 0.5. Network weights were initialized with Xavier normal distribution and a mini-batch size of 16 was used as it gave the best validation. The best performing weights were saved for segmentation performance evaluation.

The outputs obtained are shown in Fig. 2. The model input image, fully annotated, and partially annotated ground-truth data are displayed in Fig. 2a-c, respectively. White and black colors in Figs. 2b-c are the actual guidewire and background pixels, respectively. The segmentation results obtained from the proposed method are in shown Fig. 2d where white and black colors represent the pixels our method classified as guidewire and background, respectively. Overall, the method with three decoders shows mIoU of 70.81%, 67.06%, and 84.19% when implemented for the three data sets, respectively. We compared the results from our proposed method with fully-supervised counterparts. The weakly-supervised method has close performance with a mean percentage margin of  $9.24 \pm 1.51\%$  to the fully-supervised one (Fig. 2e). This is better than results obtained from three existing weakly-supervised methods (Fig. 2f-g).

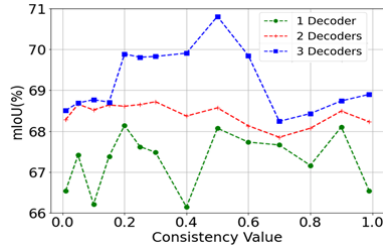


**Fig. 3:** Ablation results from different decoder numbers and consistency values.

**Table 1.** Performances of state-of-the-art models with different annotation percentage in rabbit data.

Models Used	Performance (%)			
	25%	50%	75%	Full
This Study	62.26	70.81	73.79	78.78
Omisore <i>et al</i> [29]	64.17	71.38	76.85	84.89
Badrinarayanan [34]	49.78	58.95	66.41	75.27
Zhou <i>et al</i> [6]	59.89	66.49	75.29	83.48
Chen <i>et al</i> [35]	58.63	65.57	69.76	76.24

### 3.2 Performance Comparison

We compared our method with entropy minimization, total variation, and Mumford-Shah loss regularization, which are existing weakly-supervised methods [12]. The implementation details in Section 3.1 were used without any post-segmentation steps. With respect to full supervision, the existing methods segmented the guidewire pixels with mean percentage differences of  $16.40 \pm 4.99\%$ ,  $27.64 \pm 8.18\%$ , and  $16.99 \pm 4.60\%$ , respectively. Thus, our method offers closest experience to a fully supervised method.

For further performance analysis, ablation studies were done with the rabbit data. First, we analyzed the effects of using multiple decoders. The U-Net backbone was implemented using one decoder and two decoders in different trials, and we compared their performances to the three decoder setup. The U-Net model with three decoders has best performance (Fig. 3) with average mIoU  $69.22 \pm 0.74\%$ . Using one decoder implies a model without pseudo labeling, and this gave lowest mIoU ( $67.3 \pm 0.66\%$ ). Thus, it is less effective for weakly-supervised model. The two-decoder setup, similar to pseudo labeling in [12], gave average mIoU of  $68.41 \pm .26\%$  for same trials. Thus, integrating pseudo labeling adds to segmentation performance of the proposed model.

The effect of consistency thresholds was analyzed by using different  $\lambda$  values for the shared-consistency loss in the two and three decoder setups. For training stability and transparency,  $\lambda^{d=1}$  for main decoder was fixed while random values were used for  $\lambda^{d>1}$ . We executed multiple runs with  $\lambda$  chosen between 0 and 1, and  $\sum \lambda^{d \geq 1} = 1$ . As shown in Fig. 3, the model shows some performance variations. Thus, varying  $\lambda$  values is slightly sensitive to the model’s performance. The best segmentation outputs for one, two and three decoders were obtained with  $\lambda = 0.9$ ,  $0.3$  and  $0.5$ , respectively. Lastly, we show that the proposed method works with other state-of-the-art models.

The weakly-supervised method was integrated into additional four deep networks that are used for medical image segmentation. Each network was implemented with angiogram data that have varying annotation percentages. The results obtained are in Table 1. With 25% partial annotation in each angiogram, the proposed method gave ~50% segmentation performance across all the methods. Also, performances of the weakly-supervised method are closest to those of fully-supervised at 75% annotation.

## 4 Conclusion

A weakly-supervised learning method is proposed based for guidewire segmentation



in cardiovascular angiograms. The method is implemented on a U-Net backbone with multiple decoders, and trained end-to-end with shared-consistency loss for pseudo-label generation and guidewire segmentation. Supervision signals from three decoder instances are dynamically mixed with shared consistency to spawn the pseudo labeling process and enhance the model's performance. Experiments on weakly-annotated angiograms from different catheterization studies show that the proposed multi-lateral branching method is more effective than some existing weakly supervised methods. Furthermore, we show that the proposed method has closer performances to fully-supervised counterparts. This study will be extended for real-time tracking and visualization of flexible tools used in robotic cardiac catheterization.

## References

1. Omisore O. M., *et al.*, Towards Characterization and Adaptive Compensation of Backlash in a Novel Robotic Catheter System for Cardiovascular Interventions, *IEEE Transactions on Biomedical Circuits and Systems*, 2018, 12(4): p. 824-838.
2. Naidu S. S., J. D. Abbott, J. Bagai, J. Blankenship, S. Garcia, S. N. Iqbal, P. Kaul, M. A. Gianni, A. van Rosendaal, I. van den Hoogen *et al.*, SCAI expert consensus update on best practices in the cardiac catheterization laboratory, *Catheterization and Cardiovascular Interventions*, 2021, 98(2): p. 255-276.
3. Chen C, Qin C, Qiu H, Tarroni G, Duan J, Bai W, Rueckert, Deep Learning for Cardiac Image Segmentation: A Review, *Frontiers in Cardiovascular Medicine*, 2020, 7(25).
4. Baskaran L., G. Maliakal, S. J. Al'Aref, G. Singh, Z. Xu, K. Michalak, K. Dolan, U. Gianni, A. van Rosendaal, I. van den Hoogen *et al.*, Identification and Quantification of Cardiovascular Structures From CCTA: An End-to-End, Rapid, Pixel-Wise, Deep-Learning Method, *JACC: Cardiovascular Imaging*, 2020, 13(5): p. 1163-1171.
5. Zhou Y. J., X. L. Xie, X. H. Zhou, S. Q. Liu, G. B. Bian, and Z. G. Hou, Pyramid attention recurrent networks for real-time guidewire segmentation and tracking in intraoperative X-ray fluoroscopy, *Comput Med Imaging Graph*, 2020, 83: p. 101734.
6. Zhou Y. J., *et al.*, A Real-Time Multifunctional Framework for Guidewire Morphological and Positional Analysis in Interventional X-Ray Fluoroscopy, *IEEE Transactions on Cognitive and Developmental Systems*, 2021, 13(3): p. 657-667.
7. Ronneberger O., P. Fischer, and T. Brox, U-Net: Convolutional Networks for Biomedical Image Segmentation, in *Medical Image Computing and Computer-Assisted Intervention – MICCAI 2015*, Cham, 2015, 2015//, p.234-241.
8. Zhou Z., M. M. Rahman Siddiquee, N. Tajbakhsh, and J. Liang, UNet++: A Nested U-Net Architecture for Medical Image Segmentation, in *Deep Learning in Medical Image Analysis and Multimodal Learning for Clinical Decision Support*, Cham, 2018//, p.3-11.
9. Gu Z., J. Cheng, H. Fu, K. Zhou, H. Hao, Y. Zhao, T. Zhang, S. Gao, and J. Liu, CE-Net: Context Encoder Network for 2D Medical Image Segmentation, *IEEE Transactions on Medical Imaging*, 2019, 38(10): p. 2281-2292.
10. Dhamija T., A. Gupta, S. Gupta, Anjum, R. Katarya, and G. Singh, Semantic segmentation in medical images through transfused convolution and transformer networks, *Applied Intelligence*, 2022. 10.1007/s10489-022-03642-w.
11. Calderon-Ramirez S. *et al.*, Semisupervised Deep Learning for Image Classification With Distribution Mismatch: A Survey, *IEEE Trans on Artificial Intelligence*, 2022, 3(6): 1015.
12. Luo X., M. Hu, W. Liao, S. Zhai, T. Song, G. Wang, and S. Zhang, Scribble-Supervised Medical Image Segmentation via Dual-Branch Network and Dynamically Mixed Pseudo Labels Supervision, *MICCAI 2022*, Cham, 2022, 2022//, p.528-538.
13. Shin S. Y., S. Lee, I. D. Yun, S. M. Kim, and K. M. Lee, Joint Weakly and Semi-Supervised Deep Learning for Localization and Classification of Masses in Breast Ultrasound Images, *IEEE Transactions on Medical Imaging*, 2019, 38: p. 762-774.

14. Wang J. and B. Xia, Bounding Box Tightness Prior for Weakly Supervised Image Segmentation, in MICCAI 2021, Cham, 2021, , p.526-536.
15. Qu H. *et al.*, Weakly Supervised Deep Nuclei Segmentation using Points Annotation in Histopathology Images, in MIDL2019
16. Qian H. S., Li; Xuming, He, Weakly Supervised Volumetric Segmentation via Self-taught Shape Denoising Model, in Machine Learning Research2021, p.268–285.
17. Viniavskiy O., M. Dobko, and O. Doboševych, Weakly-Supervised Segmentation for Disease Localization in Chest X-Ray Images, ArXiv, 2020, abs/2007.00748.
18. Ibrahim M. S., A. A. Badr, M. R. Abdallah, I. F. Eissa, Bounding Box Object Localization Based On Image Superpixelization, Procedia Computer Science, 2012, 13: p. 108-119.
19. Omisore O. M., *et al.*, Automatic tool segmentation and tracking during robotic intravascular catheterization for cardiac interventions, Quantitative imaging in medicine and surgery, 2021, 11 6: p. 2688-2710.
20. Girum K. B., *et al.*, Fast interactive medical image segmentation with weakly supervised deep learning method, Int J Comput Assist Radiol Surg, 2020, 15(9): p. 1437-1444.
21. Rajchl M., *et al.*, DeepCut: Object Segmentation From Bounding Box Annotations Using Convolutional Neural Networks, IEEE Trans Med Imaging, 2017, 36(2): p. 674-683.
22. Valvano G., A. Leo, and S. A. Tsafaris, Learning to Segment From Scribbles Using Multi-Scale Adversarial Attention Gates, IEEE TMI, 2021, 40(8): p. 1990-2001.
23. Zhang K., X. Zhuang, ShapePU: A New PU Learning Framework Regularized by Global Consistency for Scribble Supervised Cardiac Segmentation, in MICCAI 2022, p.162-172.
24. Zhang K. Z., Xiahai, CycleMix: A Holistic Strategy for Medical Image Segmentation From Scribble Supervision, IEEE/CVF CVPR 2022, p.11656-11665.
25. Shuwei Z. G., Wang; Xiangde, Luo; Qiang, Yue; Kang, Li; Shaoting, Zhang. (2022). PA-Seg: Learning from Point Annotations for 3D Medical Image Segmentation using Contextual Regularization and Cross Knowledge Distillation. .
26. Issam L., *et al.*, A Weakly supervised consistency-based learning method for {covid-19} segmentation in CT Images, in IEEE Winter Conference on Applications of Computer Vision, Waikoloa, HI, USA, 2021, January 3-8, 2021, p. 2452-2461.
27. Yang H., C. Shan, A. F. Kolen, P. H. Weakly-supervised learning for catheter segmentation in 3D frustum ultrasound, Comp Med Imag. Graph., 2022, 96: p. 102037.
28. Gherardini M., E. Mazomenos, A. Menciasci, and D. Stoyanov, Catheter segmentation in X-ray fluoroscopy using synthetic data and transfer learning with light U-nets, Computer Methods and Programs in Biomedicine, 2020, 192: p. 105420.
29. Omisore O. M., T. O. Akinyemi, W. Duan, W. Du, and L. Wang, Multi-Lateral Branched Network for Tool Segmentation during Robot-assisted Endovascular Interventions, IEEE Transactions on Medical Robotics & Bionics, 2024. 10.1109/TMRB.2024.3369765: p. 1.
30. Ouali Y., C. Hudelot, and M. Tami, Semi-Supervised Semantic Segmentation With Cross-Consistency Training, in 2020 IEEE/CVF CVPR, 13-19 June 2020, p.12671-12681.
31. Wu Y., M. Xu, Z. Ge, J. Cai, and L. Zhang, Semi-supervised Left Atrium Segmentation with Mutual Consistency Training, in MICCAI 2021, Cham, 2021, p.297-306.
32. Verma V., Kawaguchi, A. Lamb, J. Kannala, A. Solin, Y. Bengio, D. Lopez, Interpolation consistency training for semi-supervised learning, Neural Networks, 2022, 145: p. 90-106.
33. Zheng Y., M. J. Er, S. Shen, W. Li, Y. Li, W. Du, W. Duan, and O. M. Omisore, An Improved Image Segmentation Model based on U-Net for Interventional Intravascular Robots, 4th International Conference on Intelligent Autonomous Systems, 2021, p.84-90.
34. Badrinarayanan V., A. Kendall, and R. Cipolla, SegNet: A Deep Convolutional Encoder-Decoder Architecture for Image Segmentation, IEEE Transactions on Pattern Analysis and Machine Intelligence, 2017, 39(12): p. 2481-2495.
35. Chen L.-C., Y. Zhu, G. Papandreou, F. Schroff, and H. Adam, Encoder-Decoder with Atrous Separable Convolution for Semantic Image Segmentation, in ECCV 2018, p.833.